Commun. Comput. Phys.
doi: 10.4208/cicp.OA-2017-0212

Vol. **25**, No. 4, pp. 1127-1143
April 2019

Two Kinds of New Energy-Preserving Schemes for the Coupled Nonlinear Schrödinger Equations

Mingzhan Song[1], Xu Qian[1,2], Hong Zhang[1,3], Jingmin Xia[1,4] and Songhe Song[1,*]

[1] *College of Science and State Key Laboratory of High Performance Computing, National University of Defense Technology, Changsha, 410073, P.R. China.*
[2] *Academy of Ocean Science and Engineering, National University of Defense Technology, Changsha, 410073, P.R. China.*
[3] *Department of mathematics, Utrecht University, Utrecht, 3584CD, Netherland.*
[4] *Mathematical Institute, University of Oxford, Oxford OX2 6GG, England.*

Received 3 October 2017; Accepted (in revised version) 27 March 2018

Abstract. In this paper, we mainly propose two kinds of high-accuracy schemes for the coupled nonlinear Schrödinger (CNLS) equations, based on the Fourier pseudospectral method (FPM), the high-order compact method (HOCM) and the Hamiltonian boundary value methods (HBVMs). With periodic boundary conditions, the proposed schemes admit the global energy conservation law and converge with even-order accuracy in time. Numerical results are presented to demonstrate the accuracy, energy-preserving and long-time numerical behaviors. Compared with symplectic Runge-Kutta methods (SRKMs), the proposed schemes are assuredly more effective to preserve energy, which is consistent with our theoretical analysis.

AMS subject classifications: 37M05, 65M06

Key words: Hamiltonian boundary value methods, Fourier pseudospectral method, high-order compact method, coupled nonlinear Schrödinger equations.

1 Introduction

Since the explosion of interest in nonlinear science, the nonlinear Schrödinger equation plays a central role in a wide range of physical phenomena, including nonlinear optics [19], plasma physics [23], atomic Bose-Einstein condensates [2], etc. In order to describe two interacting nonlinear packets in dispersive or conservative systems, in 1967, the coupled nonlinear Schrödinger (CNLS) equations were firstly derived by Benney and Newell [1].

*Corresponding author. *Email addresses:* smz161619@163.com (M. Song), shsong@nudt.edu.cn (S. Song), qianxu@nudt.edu.cn (X. Qian), H.zhang@uu.nl (H. Zhang), jingmin.xia@maths.ox.ac.uk (J. Xia)

In this paper, we are mainly concerned with the CNLS equations

$$\begin{cases} \mathrm{i}\phi_t+\phi_{xx}+(|\phi|^2+\beta|\psi|^2)\phi=0, \\ \mathrm{i}\psi_t+\psi_{xx}+(|\psi|^2+\beta|\phi|^2)\psi=0, \end{cases} \tag{1.1}$$

with suitable initial data and periodic boundary conditions. Here, $\phi(x,t)$ and $\psi(x,t)$, $(x,t)\in[x_L,x_R]\times[0,T]$, are complex envelopes of two wave packets, β is the coupling constant and i is the imaginary unit. Due to the intrinsic stability of equations, solitons could be formed when the nonlinear term exactly balances the wave packet dispersion and their dynamics have appeared in many important applications [27, 29]. Therefore, the signification about solitons of the CNLS equations (1.1) has been widely acknowledged.

So far, numerous researches have been conducted to solve the CNLS equations. Based on the finite difference method, Ismail and Alamri have achieved linearly implicit conservative scheme [20] and fourth-order explicit scheme [21]. Both of them could preserve discrete energy exactly. Kurtinaitis and Ivanauska [24] employed explicit, implicit, Crank-Nicolson type and Hopsotch type finite difference scheme, respectively, to simulate the dynamics of the 3-CNLS equations. In [22], the Galerkin method was utilized for the CNLS equations. In [4], the authors discussed how to apply the differential transformation method to solve the CNLS equations. Furthermore, Bao et al. [3] simulated the bright and dark soliton solutions of the CNLS system successfully by using the time-splitting pseudospectral method.

In recent decades, it has been widely convinced that structure-preserving methods, which are able to preserve the intrinsic properties of the original system, could achieve long-time high precision simulation in most cases. Therefore, many important results were subsequently reported, such as symplectic Runge-Kutta methods (SRKMs) [18,31], multi-symplectic methods [15,28] and semi-explicit and explicit multi-symplectic methods [30,32]. In addition, energy-preserving methods, including discrete gradient method [26], local energy-preserving method [17], average vector field method [16] and Hamiltonian boundary value methods (HBVMs), were widely applied for numerical simulation as well. Due to its remarkable energy-preserving property, the HBVMs has attracted much attention since it was first proposed for ODEs by Brugnano et al. [5, 6] in 2010. In [7], the efficient implementation of the HBVMs was fully discussed. Then Brugnano and Sun [8] further proposed a multiple invariants conserving method for Hamiltonian ODEs. Recently, this method was generalised to solve semilinear wave equations [9], nonlinear Schrödinger equation [12, 13] and other Hamiltonian PDEs [10, 11]. To the best of our knowledge, there exists no report about the application of the HBVMs for the CNLS equations at the moment, so we combine this energy-preserving method with the Fourier pseudospectral method (FPM) [14] and the high-order compact method (HOCM) [25] to construct two kinds of numerical schemes.

As is well known, we can rewrite the CNLS equations (1.1) as the infinite-dimensional Hamiltonian system

$$\frac{\partial z}{\partial t}=J\frac{\delta\mathcal{H}}{\delta z}, \tag{1.2}$$

where $z=(\phi,\ \psi)^{\mathrm{T}}$, and J is a constant linear skew-symmetric operator. According to the variational derivative formula [16]

$$\frac{\delta\mathcal{H}}{\delta u}=\frac{\partial H}{\partial u}-\partial_x\left(\frac{\partial H}{\partial u_x}\right)+\partial_x^2\left(\frac{\partial H}{\partial u_{xx}}\right)-\cdots, \tag{1.3}$$

we have

$$\mathcal{H}[\phi,\psi](t)=\int_\Omega H(x,t)\mathrm{d}x=\int_\Omega\left[\frac{1}{4}(|\phi|^4+|\psi|^4)-\frac{1}{2}(|\phi_x|^2+|\psi_x|^2)+\frac{\beta}{2}|\phi|^2|\psi|^2\right]\mathrm{d}x. \tag{1.4}$$

Here, the Hamiltonian $\mathcal{H}$ also represents the global energy of the CNLS system (1.1), meanwhile, it could be intrinsically preserved,

$$\frac{\mathrm{d}\mathcal{H}}{\mathrm{d}t}=\frac{\delta\mathcal{H}}{\delta z}\frac{\partial z}{\partial t}=\frac{\delta\mathcal{H}}{\delta z}J\frac{\delta\mathcal{H}}{\delta z}=0.$$

By letting $\phi(x,t)=q_1(x,t)+\mathrm{i}q_2(x,t)$ and $\psi(x,t)=q_3(x,t)+\mathrm{i}q_4(x,t)$, the Hamiltonian system (1.2) can be expanded as the real-valued equations

$$\begin{cases}\frac{\partial q_1}{\partial t}=-\frac{\partial^2 q_2}{\partial x^2}-\left((q_1^2+q_2^2)+\beta(q_3^2+q_4^2)\right)q_2,\\ \frac{\partial q_2}{\partial t}=\ \ \frac{\partial^2 q_1}{\partial x^2}+\left((q_1^2+q_2^2)+\beta(q_3^2+q_4^2)\right)q_1,\\ \frac{\partial q_3}{\partial t}=-\frac{\partial^2 q_4}{\partial x^2}-\left((q_3^2+q_4^2)+\beta(q_1^2+q_2^2)\right)q_4,\\ \frac{\partial q_4}{\partial t}=\ \ \frac{\partial^2 q_3}{\partial x^2}+\left((q_3^2+q_4^2)+\beta(q_1^2+q_2^2)\right)q_3,\end{cases} \tag{1.5}$$

that is,

$$\begin{pmatrix}\frac{\partial q_1}{\partial t}\\ \frac{\partial q_2}{\partial t}\\ \frac{\partial q_3}{\partial t}\\ \frac{\partial q_4}{\partial t}\end{pmatrix}=\begin{pmatrix}0&-1&0&0\\1&0&0&0\\0&0&0&-1\\0&0&1&0\end{pmatrix}\begin{pmatrix}\frac{\partial^2 q_1}{\partial x^2}+\left((q_1^2+q_2^2)+\beta(q_3^2+q_4^2)\right)q_1\\ \frac{\partial^2 q_2}{\partial x^2}+\left((q_1^2+q_2^2)+\beta(q_3^2+q_4^2)\right)q_2\\ \frac{\partial^2 q_3}{\partial x^2}+\left((q_3^2+q_4^2)+\beta(q_1^2+q_2^2)\right)q_3\\ \frac{\partial^2 q_4}{\partial x^2}+\left((q_3^2+q_4^2)+\beta(q_1^2+q_2^2)\right)q_4\end{pmatrix}. \tag{1.6}$$

Meanwhile, because of the periodic boundary conditions, the Hamiltonian $\mathcal{H}$ (1.4) can be rewritten as

$$\begin{aligned}\mathcal{H}[q_1,q_2,q_3,q_4](t)=\int_\Omega\Big[&\frac{1}{4}(q_1^2+q_2^2)^2+\frac{1}{4}(q_3^2+q_4^2)^2+\frac{\beta}{2}(q_1^2+q_2^2)(q_3^2+q_4^2)\\&+\frac{1}{2}(q_1q_{1xx}+q_2q_{2xx}+q_3q_{3xx}+q_4q_{4xx})\Big]\mathrm{d}x.\end{aligned} \tag{1.7}$$

The rest of the paper is arranged as follows. In the next section, we transform the infinite-dimensional Hamiltonian system into the finite-dimensional Hamiltonian system by using the FPM and the HOCM. Hereafter, energy-preserving schemes are constructed for the CNLS equations based on the HBVMs in Section 3. In Section 4, numerical experiments are performed to testify the effectiveness of the proposed schemes. Finally, conclusions are made in Section 5.

2 Space-discretization by the FPM and the HOCM

In this section, two different spatial discretizations, the FPM and the HOCM, are introduced. Both of them are natural to work on a bounded domain $[x_L,x_R]$ and an uniform grid (x_i,t_j) with $x_i=x_L+i\Delta x$ $(i=0,1,\cdots,M-1)$ and $t_j=j\Delta t$ $(j=0,1,\cdots,N)$ is considered.

Firstly, based on the standard Fourier pseudospectral formulation, the FPM [14] could construct the spectral differentiation matrices D_1 and D_2, which are widely used in discretization of differential operators ∂_x and ∂_{xx},

$$(D_1)_{j,l}=\begin{cases}\frac{1}{2}(-1)^{j+l}\mu\cot(\mu\frac{x_j-x_l}{2}), & j\neq l,\\ 0, & j=l,\end{cases}$$

$$(D_2)_{j,l}=\begin{cases}\frac{1}{2}(-1)^{j+l+1}\mu^2\csc^2(\mu\frac{x_j-x_l}{2}), & j\neq l,\\ -\mu^2\frac{N^2+2}{12}, & j=l,\end{cases}$$

where $j,l=1,\cdots,M$ and $\mu=2\pi/L$, $L=x_R-x_L$. Actually, the biggest advantage of this method is that it could achieve spectral accuracy in spatial direction.

Alternatively, we can apply the HOCM, which is beneficial to reduce the computational cost, to discrete differential operators as well. Considering the discretization of the first-order derivative, we have the formula [25]

$$\beta f'_{i-2}+\alpha f'_{i-1}+f'_i+\alpha f'_{i+1}+\beta f'_{i+2}=c\frac{f_{i+3}-f_{i-3}}{6\Delta x}+b\frac{f_{i+2}-f_{i-2}}{4\Delta x}+a\frac{f_{i+1}-f_{i-1}}{2\Delta x}. \tag{2.1}$$

When the coefficients are chosen as $\alpha=\frac{1}{3}$, $\beta=0$, $a=\frac{14}{9}$, $b=\frac{1}{9}$, $c=0$, the truncation error $\frac{4}{7!}(\Delta x)^6 f^{(7)}$ vanishes and the formula (2.1) is formally sixth-order accurate in space. Under the periodic boundary condition, the first-order differentiation matrix can be written as $\tilde{D}_1=A^{-1}B$,

$$A=\frac{1}{3}\begin{pmatrix}3&1&&&1\\1&3&1&&\\&\ddots&\ddots&\ddots&\\&&1&3&1\\1&&&1&3\end{pmatrix},\quad B=\frac{1}{36\Delta x}\begin{pmatrix}0&28&1&&&-1&-28\\-28&0&28&1&&&-1\\-1&-28&0&28&1&&\\0&\ddots&\ddots&\ddots&\ddots&\ddots&\\&&-1&-28&0&28&1\\1&&&-1&-28&0&28\\28&1&&&-1&-28&0\end{pmatrix},$$

and the second-order differentiation matrix could be naturally obtained as $\tilde{D}_2=\tilde{D}_1^2$. Obviously, this method is able to construct sixth-order compact scheme in spatial direction.

More importantly, these two space discretization methods are able to guarantee that the first-order differentiation matrices are skew-symmetric and the second-order differentiation matrices are symmetric. This is the key to preserve global energy or Hamiltonian exactly. In following text, we first use D_1 and D_2 to construct numerical schemes

based on the FPM, and the other numerical schemes based on the HOCM can be obtained easily by replacing D_1, D_2 with $\tilde{D}_1$, $\tilde{D}_2$.

After the space-discretization, the following semi-discrete Hamiltonian system can be obtained as

$$\begin{cases} \dot{\mathbf{q}}_1 = -D_2\mathbf{q}_2 - \big((\mathbf{q}_1.^2+\mathbf{q}_2.^2)+\beta(\mathbf{q}_3.^2+\mathbf{q}_4.^2)\big).*\mathbf{q}_2, \\ \dot{\mathbf{q}}_2 = \quad D_2\mathbf{q}_1 + \big((\mathbf{q}_1.^2+\mathbf{q}_2.^2)+\beta(\mathbf{q}_3.^2+\mathbf{q}_4.^2)\big).*\mathbf{q}_1, \\ \dot{\mathbf{q}}_3 = -D_2\mathbf{q}_4 - \big((\mathbf{q}_3.^2+\mathbf{q}_4.^2)+\beta(\mathbf{q}_1.^2+\mathbf{q}_2.^2)\big).*\mathbf{q}_4, \\ \dot{\mathbf{q}}_4 = \quad D_2\mathbf{q}_3 + \big((\mathbf{q}_3.^2+\mathbf{q}_4.^2)+\beta(\mathbf{q}_1.^2+\mathbf{q}_2.^2)\big).*\mathbf{q}_3, \end{cases} \tag{2.2}$$

where $\mathbf{q}_i(t)=\big(q_{ij}(t)\big)_{M\times 1}$ (i=1,2,3,4, j=0,$\cdots$,$M-1$), $\mathbf{q}_m.^2=(q_{m0}\times q_{m0},\cdots,q_{m,M-1}\times q_{m,M-1})^{\mathrm{T}}$ and $\mathbf{q}_m.*\mathbf{q}_n=(q_{m0}\times q_{n0},\cdots,q_{m,M-1}\times q_{n,M-1})^{\mathrm{T}}$, m,n=1,2,3,4. Meanwhile, the discrete form of the Hamiltonian $\mathcal{H}$ (1.7) is

$$\begin{aligned} H(\mathbf{q}_1,\mathbf{q}_2,\mathbf{q}_3,\mathbf{q}_4) =& \Delta x\sum_{j=0}^{N-1}\left(\frac{1}{4}(q_{1j}^2+q_{2j}^2)^2+\frac{1}{4}(q_{3j}^2+q_{4j}^2)^2+\frac{1}{2}\beta(q_{1j}^2+q_{2j}^2)(q_{3j}^2+q_{4j}^2)\right) \\ &+\frac{1}{2}\Delta x\Big(\mathbf{q}_1^{\mathrm{T}}D_2\mathbf{q}_1+\mathbf{q}_2^{\mathrm{T}}D_2\mathbf{q}_2+\mathbf{q}_3^{\mathrm{T}}D_2\mathbf{q}_3+\mathbf{q}_4^{\mathrm{T}}D_2\mathbf{q}_4\Big). \end{aligned} \tag{2.3}$$

By introducing

$$\mathbf{J}=\frac{1}{\Delta x}\begin{pmatrix} 0 & -\mathbf{I} & 0 & 0 \\ \mathbf{I} & 0 & 0 & 0 \\ 0 & 0 & 0 & -\mathbf{I} \\ 0 & 0 & \mathbf{I} & 0 \end{pmatrix}, \quad \mathbf{z}=\begin{pmatrix} \mathbf{q}_1 \\ \mathbf{q}_2 \\ \mathbf{q}_3 \\ \mathbf{q}_4 \end{pmatrix},$$

Eq. (2.2) can be rewritten as

$$\dot{\mathbf{z}}=f(\mathbf{z})=\mathbf{J}\nabla H(\mathbf{z}), \tag{2.4}$$

where ∇ is the gradient operator. Consequently,

$$\frac{\mathrm{d}H(\mathbf{z})}{\mathrm{d}t}=\nabla H(\mathbf{z})^{\mathrm{T}}\dot{\mathbf{z}}=\nabla H(\mathbf{z})^{\mathrm{T}}\mathbf{J}\nabla H(\mathbf{z})\equiv 0.$$

Thus, $H(\mathbf{z})$ is still intrinsically preserved after space-discretization. In the following text, we will focus on the semi-discrete problem (2.4).

3 Hamiltonian boundary value methods for the CNLS equations

In this section, the HBVMs will be used for the full discretization of the CNLS equations. To achieve one-step approximation over $[t_0,t_0+\Delta t]$, we take the scaled and shifted Legendre polynomials in the interval $[0,1]$, $P_i(t)$, satisfy the recurrence formula:

$$\begin{aligned} &P_0(t)=1, \quad P_1(t)=\sqrt{3}(2t-1), \\ &P_{i+1}(t)=(2t-1)\frac{2i+1}{i+1}\sqrt{\frac{2i+3}{2i+1}}P_i(t)-\frac{i}{i+1}\sqrt{\frac{2i+3}{2i-1}}P_{i-1}(t), \quad i=1,2,\cdots. \end{aligned}$$

Following the approach in [7], the right-hand side of the system (2.4) can be expanded in the interval $[0,\Delta t]$, as

$$\dot{\mathbf{z}}(t_0+\tau\Delta t)=\sum_{j=0}^{\infty}\gamma_j(\mathbf{z})P_j(\tau),\quad \tau\in[0,\,1], \tag{3.1}$$

where $\gamma_j(\mathbf{z})=\langle f(\mathbf{z}),P_j(\tau)\rangle$ is the Fourier coefficient. By truncating the series, we set $\dot{\boldsymbol{\sigma}}(t)$ as the approximation of $\dot{\mathbf{z}}(t)$ over $[t_0,t_0+\Delta t]$,

$$\dot{\boldsymbol{\sigma}}(t_0+\tau\Delta t)=\sum_{j=0}^{r-1}\gamma_j(\boldsymbol{\sigma})P_j(\tau),\quad \tau\in[0,\,1]. \tag{3.2}$$

Then, the approximation polynomial $\boldsymbol{\sigma}(t)$ of true solution $\mathbf{z}(t)$ is taken as

$$\boldsymbol{\sigma}(t_0+\tau\Delta t)=\boldsymbol{\sigma}_0+\Delta t\sum_{j=0}^{r-1}\gamma_j(\boldsymbol{\sigma})\int_0^{\tau}P_j(x)dx,\quad \tau\in[0,\,1], \tag{3.3}$$

where $\boldsymbol{\sigma}_0=\boldsymbol{\sigma}(t_0)=\mathbf{z}(t_0)$. Consequently,

$$\begin{aligned}H(\boldsymbol{\sigma}(t_0+\Delta t))-H((\boldsymbol{\sigma}(t_0))&=\Delta t\int_0^1\nabla H((\boldsymbol{\sigma}(t_0+\tau\Delta t))^{\mathrm{T}}\dot{\boldsymbol{\sigma}}(t_0+\tau\Delta t)d\tau\\&=\Delta t\sum_{j=0}^{r-1}\left(\int_0^1P_j(\tau)\nabla H((\boldsymbol{\sigma}(t_0+\tau\Delta t))d\tau\right)^{\mathrm{T}}\gamma_j(\boldsymbol{\sigma}).\end{aligned} \tag{3.4}$$

Based on the rule of inner product, we set

$$\gamma_j(\boldsymbol{\sigma})=\int_0^1P_j(\tau)\mathbf{J}\nabla H((\boldsymbol{\sigma}(t_0+\tau\Delta t))d\tau,\quad j=0,\cdots,r-1,$$

where $\mathbf{J}$ is skew-symmetric. Then the Hamiltonian can be preserved theoretically,

$$\begin{aligned}&H((\boldsymbol{\sigma}(t_0+\Delta t))-H((\boldsymbol{\sigma}(t_0))\\=&\Delta t\sum_{j=0}^{r-1}\left(\int_0^1P_j(\tau)\nabla H((\boldsymbol{\sigma}(t_0+\tau\Delta t))dc\right)^{\mathrm{T}}\int_0^1P_j(\tau)\mathbf{J}\nabla H((\boldsymbol{\sigma}(t_0+\tau\Delta t))d\tau\\=&\Delta t\sum_{j=0}^{r-1}\left(\int_0^1P_j(\tau)\nabla H((\boldsymbol{\sigma}(t_0+\tau\Delta t))d\tau\right)^{\mathrm{T}}\mathbf{J}\left(\int_0^1P_j(\tau)\nabla H((\boldsymbol{\sigma}(t_0+\tau\Delta t))d\tau\right)=0.\end{aligned} \tag{3.5}$$

For the integral of $\gamma_j(\boldsymbol{\sigma})$, the Gauss-Legendre quadrature formula is applied,

$$\gamma_j=\sum_{l=1}^{k}\alpha_lP_j(c_l)\mathbf{J}\nabla H((\sigma(t_0+c_l\Delta t))+E_j(\Delta t), \tag{3.6}$$

where c_i and α_i $(i=1,\cdots,k)$ are the distinct abscissae and corresponding weights, respectively, and $E_j(\Delta t)$ denotes the error of the numerical integration formula. Ignoring the quadrature error in Eq. (3.6) and the truncation error in Eq. (3.2) temporarily, we have

$$\dot{\boldsymbol{\sigma}}(t_0+c_i\Delta t)=\sum_{j=0}^{r-1}P_j(c_i)\left(\sum_{l=1}^{k}\alpha_l P_j(c_l)\mathbf{J}\nabla H(\boldsymbol{\sigma}(t_0+c_l\Delta t))\right), \tag{3.7}$$

and

$$\boldsymbol{\sigma}(t_0+c_i\Delta t)=\boldsymbol{\sigma}_0+\Delta t\sum_{l=1}^{k}\alpha_l\left(\sum_{j=0}^{r-1}a_{ij}P_j(c_l)\right)\mathbf{J}\nabla H(\boldsymbol{\sigma}(t_0+c_l\Delta t)), \tag{3.8}$$

where $a_{ij}=\int_0^{c_i}P_j(t)dt$ $(i=1,\cdots,k,\ j=0,\cdots,r-1)$. According to Eq. (3.8), the approximation to $\mathbf{z}(t_0+\Delta t)$ is given by

$$\boldsymbol{\sigma}(t_0+\Delta t)=\boldsymbol{\sigma}_0+\Delta t\sum_{i=1}^{k}\alpha_i\mathbf{J}\nabla H(\boldsymbol{\sigma}(t_n+c_i\Delta t)). \tag{3.9}$$

Concerning the accuracy of such an approximation, it can be proved (see, e.g., [7]) that: when $k\geq s$ and $\boldsymbol{\sigma}(t_0+\Delta t)$ is the approximation of $\mathbf{z}(t_0+\Delta t)$ provided by Eq. (3.9), then

$$\mathbf{z}(t_0+\Delta t)-\boldsymbol{\sigma}(t_0+\Delta t)=\mathcal{O}(\Delta t^{2r+1}). \tag{3.10}$$

Concerning the Hamiltonian error, which depends on the quadrature error in Eq. (3.6), according to [7], it can be proved that

$$H(\boldsymbol{\sigma}(t_0+\Delta t))-H(\boldsymbol{\sigma}(t_0))=0, \tag{3.11}$$

when H is a polynomial and its degree $v\leq 2k/r$. Conversely

$$H(\boldsymbol{\sigma}(t_0+\Delta t))-H(\boldsymbol{\sigma}(t_0))=\mathcal{O}(\Delta t^{2k+1}). \tag{3.12}$$

In the present case, since the Hamiltonian (2.3) is a polynomial of degree 4, any HBVMs(k,r) ($k\geq 2r$) will be convergent of order $2r$ and energy-preserving. For the semi-discrete CNLS equations (2.2), the first step of application of the energy-preserving schemes can be written as

$$\begin{cases}
\frac{1}{\Delta t}\left(\mathbf{q}_1^1-\mathbf{q}_1^0\right)=-\sum_{i=1}^{k}\alpha_i\left(D_2Q_{2i}+\left(\left(Q_{1i}.^2+Q_{2i}.^2\right)+\beta\left(Q_{3i}.^2+Q_{4i}.^2\right)\right).*Q_{2i}\right),\\
\frac{1}{\Delta t}\left(\mathbf{q}_2^1-\mathbf{q}_2^0\right)=\ \ \sum_{i=1}^{k}\alpha_i\left(D_2Q_{1i}+\left(\left(Q_{1i}.^2+Q_{2i}.^2\right)+\beta\left(Q_{3i}.^2+Q_{4i}.^2\right)\right).*Q_{1i}\right),\\
\frac{1}{\Delta t}\left(\mathbf{q}_3^1-\mathbf{q}_3^0\right)=-\sum_{i=1}^{k}\alpha_i\left(D_2Q_{4i}+\left(\left(Q_{1i}.^2+Q_{2i}.^2\right)+\beta\left(Q_{3i}.^2+Q_{4i}.^2\right)\right).*Q_{4i}\right),\\
\frac{1}{\Delta t}\left(\mathbf{q}_4^1-\mathbf{q}_4^0\right)=\ \ \sum_{i=1}^{k}\alpha_i\left(D_2Q_{3i}+\left(\left(Q_{1i}.^2+Q_{2i}.^2\right)+\beta\left(Q_{3i}.^2+Q_{4i}.^2\right)\right).*Q_{3i}\right),
\end{cases} \tag{3.13}$$

where

$$\begin{pmatrix} \mathbf{q}_1^0 \\ \mathbf{q}_2^0 \\ \mathbf{q}_3^0 \\ \mathbf{q}_4^0 \end{pmatrix} := \sigma_0, \quad \begin{pmatrix} \mathbf{q}_1^1 \\ \mathbf{q}_2^1 \\ \mathbf{q}_3^1 \\ \mathbf{q}_4^1 \end{pmatrix} := \sigma(t_0+\Delta t), \quad \begin{pmatrix} Q_{1i} \\ Q_{2i} \\ Q_{3i} \\ Q_{4i} \end{pmatrix} := \sigma(t_0+c_i\Delta t), \quad ,i=1,\cdots,k,$$

and $\sigma(t_0+c_i\Delta t)$ is defined according to (3.8). Then the following steps of numerical iteration are similar as before. Here, we mainly consider the situations of $k=2r$, $r=1,2,3,$, and construct second-order, fourth-order and sixth-order schemes in time, respectively. Actually, when $k=r$, scheme (3.13) reduces to r-stage Gauss-Legendre SRKM and fails to preserve energy exactly, whereas the HBVMs(k,r) are all equivalent, up to round-off errors, for $k\geq 2r$. Especially, when $k=r=1$, the HBVM is equivalent to the symplectic implicit mid-point method,

$$\begin{cases} \frac{1}{\Delta t}(\mathbf{q}_1^1-\mathbf{q}_1^0) = -D_2\mathbf{q}_2^{\frac{1}{2}} - \left((\mathbf{q}_1^{\frac{1}{2}}).^2+(\mathbf{q}_2^{\frac{1}{2}}).^2+\beta(\mathbf{q}_3^{\frac{1}{2}}).^2+\beta(\mathbf{q}_4^{\frac{1}{2}}).^2\right).*\mathbf{q}_2^{\frac{1}{2}}, \\ \frac{1}{\Delta t}(\mathbf{q}_2^1-\mathbf{q}_2^0) = \quad D_2\mathbf{q}_1^{\frac{1}{2}} + \left((\mathbf{q}_1^{\frac{1}{2}}).^2+(\mathbf{q}_2^{\frac{1}{2}}).^2+\beta(\mathbf{q}_3^{\frac{1}{2}}).^2+\beta(\mathbf{q}_4^{\frac{1}{2}}).^2\right).*\mathbf{q}_1^{\frac{1}{2}}, \\ \frac{1}{\Delta t}(\mathbf{q}_3^1-\mathbf{q}_3^0) = -D_2\mathbf{q}_4^{\frac{1}{2}} - \left((\mathbf{q}_3^{\frac{1}{2}}).^2+(\mathbf{q}_4^{\frac{1}{2}}).^2+\beta(\mathbf{q}_1^{\frac{1}{2}}).^2+\beta(\mathbf{q}_2^{\frac{1}{2}}).^2\right).*\mathbf{q}_4^{\frac{1}{2}}, \\ \frac{1}{\Delta t}(\mathbf{q}_4^1-\mathbf{q}_4^0) = \quad D_2\mathbf{q}_3^{\frac{1}{2}} + \left((\mathbf{q}_3^{\frac{1}{2}}).^2+(\mathbf{q}_4^{\frac{1}{2}}).^2+\beta(\mathbf{q}_1^{\frac{1}{2}}).^2+\beta(\mathbf{q}_2^{\frac{1}{2}}).^2\right).*\mathbf{q}_3^{\frac{1}{2}}, \end{cases} \tag{3.14}$$

where $\mathbf{q}_i^{\frac{1}{2}} = \frac{1}{2}(\mathbf{q}_i^0+\mathbf{q}_i^1)$, $i=1,2,3,4$.

Furthermore, the other kind of scheme, using the HOCM for space-discretization, could be constructed based on scheme (3.13) by replacing D_2 with $\tilde{D}_2$,

$$\begin{cases} \frac{1}{\Delta t}(\mathbf{q}_1^1-\mathbf{q}_1^0) = -\sum_{i=1}^k \alpha_i\left(\tilde{D}_2Q_{2i}+\left((Q_{1i}.^2+Q_{2i}.^2)+\beta(Q_{3i}.^2+Q_{4i}.^2)\right).*Q_{2i}\right), \\ \frac{1}{\Delta t}(\mathbf{q}_2^1-\mathbf{q}_2^0) = \quad \sum_{i=1}^k \alpha_i\left(\tilde{D}_2Q_{1i}+\left((Q_{1i}.^2+Q_{2i}.^2)+\beta(Q_{3i}.^2+Q_{4i}.^2)\right).*Q_{1i}\right), \\ \frac{1}{\Delta t}(\mathbf{q}_3^1-\mathbf{q}_3^0) = -\sum_{i=1}^k \alpha_i\left(\tilde{D}_2Q_{4i}+\left((Q_{1i}.^2+Q_{2i}.^2)+\beta(Q_{3i}.^2+Q_{4i}.^2)\right).*Q_{4i}\right), \\ \frac{1}{\Delta t}(\mathbf{q}_4^1-\mathbf{q}_4^0) = \quad \sum_{i=1}^k \alpha_i\left(\tilde{D}_2Q_{3i}+\left((Q_{1i}.^2+Q_{2i}.^2)+\beta(Q_{3i}.^2+Q_{4i}.^2)\right).*Q_{3i}\right). \end{cases} \tag{3.15}$$

4 Numerical experiments

The main purpose of this section is to assess high-accuracy, energy-preserving and long-time numerical behaviors of the proposed schemes (3.13) and (3.15) with $k=2r$, $r=1,2,3$, by simulating the evolution of solitons. In the following numerical experiments, unless the content is stated, scheme (3.13) is mainly applied.

4.1 Single soliton

In this experiment, we take $\beta=1$ and the initial conditions as

$$\phi(x,0)=\psi(x,0)=\text{sech}(x)\exp(\text{i}x), \quad -30\leqslant x\leqslant 30. \tag{4.1}$$

First, we discuss the situation of $r=1$. The L_2, L_∞ solution errors and the convergence orders in time with $\Delta x=0.2$ are exhibited in Table 1 and Table 2. Obviously, both of the two numerical solutions converge to the exact solution with second order in time and their solution errors are very close. Then, with different grids, Table 3 presents different maximum energy errors for $k=1$ and $k=2$ in $t\in[0,10]$. By comparison, the HBVM(1,1) can only keep energy in some degree, whereas the HBVM(2,1) has marked effectiveness of energy-preserving, even if the grid is crude. Fig. 1 shows the propagation of the single soliton in $t\in[0,200]$. From this figure, we find that the waveforms of ϕ and ψ are always

Table 1: The convergence orders in time of scheme (3.13) with $r=1$, $k=2$ at $t=1$.

	Δt	L_2 error	order	L_∞ error	order
ϕ	0.005	4.2187×10^{-4}	-	2.9214×10^{-4}	-
	0.0025	1.0429×10^{-4}	2.0162	7.2156×10^{-5}	2.0175
	0.00125	2.4833×10^{-5}	2.0425	1.7179×10^{-5}	2.0705
ψ	0.005	4.2187×10^{-4}	-	2.9214×10^{-4}	-
	0.0025	1.0429×10^{-4}	2.0162	7.2156×10^{-5}	2.0175
	0.00125	2.4833×10^{-5}	2.0425	1.7179×10^{-5}	2.0705

Table 2: The convergence orders in time of scheme (3.13) with $r=1$, $k=1$ at $t=1$.

	Δt	L_2 error	order	L_∞ error	order
ϕ	0.005	3.9168×10^{-4}	-	3.0801×10^{-4}	-
	0.0025	9.6833×10^{-5}	2.0161	7.6079×10^{-5}	2.0174
	0.00125	2.3059×10^{-5}	2.0702	1.8113×10^{-5}	2.0705
ψ	0.005	3.9168×10^{-4}	-	3.0801×10^{-4}	-
	0.0025	9.6833×10^{-5}	2.0161	7.6079×10^{-5}	2.0174
	0.00125	2.3059×10^{-5}	2.0702	1.8113×10^{-5}	2.0705

Table 3: Maximum energy errors of scheme (3.13) in $t\in[0,10]$ with $r=1$.

Δx	Δt	$k=1$	$k=2$
0.8	0.08	1.0422×10^{-1}	5.4783×10^{-12}
0.8	0.04	3.8533×10^{-2}	1.4937×10^{-11}
0.4	0.02	4.6107×10^{-5}	1.5365×10^{-13}
0.2	0.005	1.7368×10^{-7}	1.2523×10^{-13}

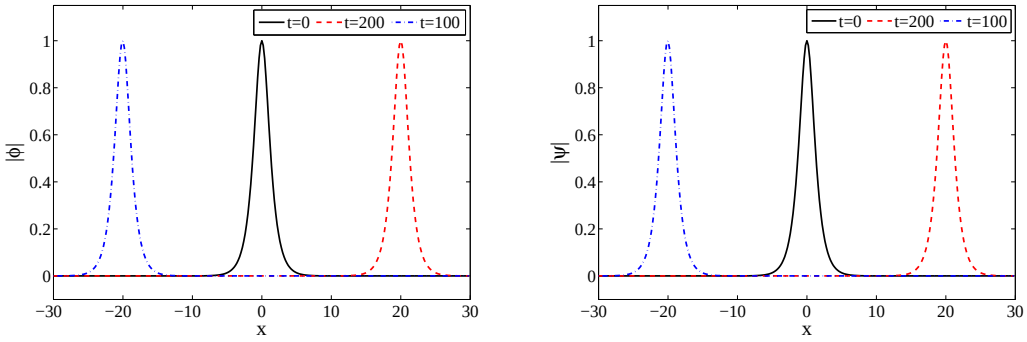

Figure 1: The waveform of the initial conditions and numerical solutions of scheme (3.13) with $r=1$, $k=2$ at $t=100$ and $t=200$ ($\Delta x=0.2$, $\Delta t=0.005$).

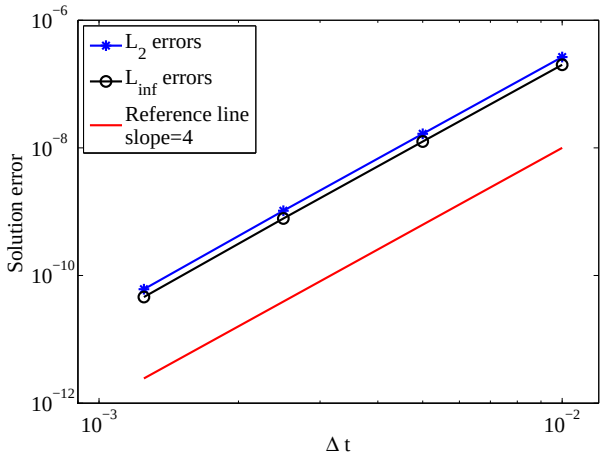

Figure 2: The convergence orders in time of scheme (3.13) with $r=2$, $k=4$ at $t=1$ ($\Delta x=0.2$).

the same at $t=0$, $t=100$ and $t=200$. This is why the solution errors of ϕ and ψ have no differences in Table 1.

Second, we set $r=2$. In Fig. 2, the convergence orders in time of scheme (3.13) with $k=4$ are observed. As is shown, the numerical results are consistent with the theoretical estimation. That is, the convergence order in time is four. Maximum energy errors of scheme (3.13) with different grid and different k are listed in Table 4. Energy-preserving scheme ($k=4$) certainly has better performance in terms of the energy error. However, if the grid is small enough, all of them could achieve practical energy-preserving in this experiment. Moreover, we also find when $k=4$, the energy error of $\Delta x=0.4$, $\Delta t=0.02$ is smaller than that of $\Delta x=0.2$, $\Delta t=0.01$. In fact, smaller grid renders larger number of the iterations and more accumulated errors for simulation. So this may cause some special cases, especially when the energy errors are approaching to the machine precision. Here, taking the same parameters, the solution errors and energy errors of scheme (3.15) are

Table 4: Maximum energy errors of scheme (3.13) in $t\in[0,10]$ with $r=2$.

Δx	Δt	$k=2$	$k=4$
1	0.1	9.1290×10^{-4}	1.0836×10^{-13}
1	0.05	5.7804×10^{-5}	1.6076×10^{-13}
0.8	0.08	2.2236×10^{-3}	1.4300×10^{-13}
0.8	0.04	1.4212×10^{-4}	3.3129×10^{-13}
0.4	0.04	5.6847×10^{-7}	3.9968×10^{-14}
0.4	0.02	6.2472×10^{-8}	3.7303×10^{-14}
0.2	0.01	3.8813×10^{-13}	1.1546×10^{-13}

Table 5: The space accuracy test of scheme (3.13) with $r=2$, $k=4$ at $t=1$ ($\Delta t=0.00025$).

	N	L_2 error	L_∞ error
ϕ	150	2.3899×10^{-3}	1.5809×10^{-4}
	300	3.9876×10^{-9}	2.9470×10^{-10}
	600	9.9190×10^{-14}	6.9156×10^{-13}
ψ	150	2.3899×10^{-3}	1.5809×10^{-4}
	300	3.9876×10^{-9}	2.9470×10^{-10}
	600	9.9190×10^{-14}	6.9156×10^{-13}

Table 6: The space accuracy test of scheme (3.15) with $r=2$, $k=4$ at $t=1$ ($\Delta t=0.00025$).

	N	L_2 error	order	L_∞ error	order
ϕ	300	5.1920×10^{-4}	-	2.9426×10^{-4}	-
	600	7.8994×10^{-6}	6.0398	4.3411×10^{-6}	6.0829
	1200	1.1990×10^{-7}	6.0418	6.5889×10^{-8}	6.0419
ψ	300	5.1920×10^{-4}	-	2.9426×10^{-4}	-
	600	7.8994×10^{-6}	6.0398	4.3411×10^{-6}	6.0829
	1200	1.1990×10^{-7}	6.0418	6.5889×10^{-8}	6.0419

almost the same as those in Fig. 2 and Table 4. Then the convergence orders in space are considered with $\Delta t=0.00025$. From Table 5 and Table 6, we find that, as Δx becomes smaller, the solution errors of scheme (3.13) decrease in an exponential rate and the numerical solution of scheme (3.15) converges in sixth-order in space. However, when the time grid is very small, under the same space grid, the solution errors of scheme (3.15) are obviously larger than that of scheme (3.13).

At last, we let $r=3$. Similarly, Fig. 3 shows that the sixth-order convergent rate in time of scheme (3.13) with $k=6$, which still coincides with our theoretical assertions. Table 7 presents maximum energy errors in $t\in[0,10]$, which could acquire the same conclusion like the situation of $r=2$.

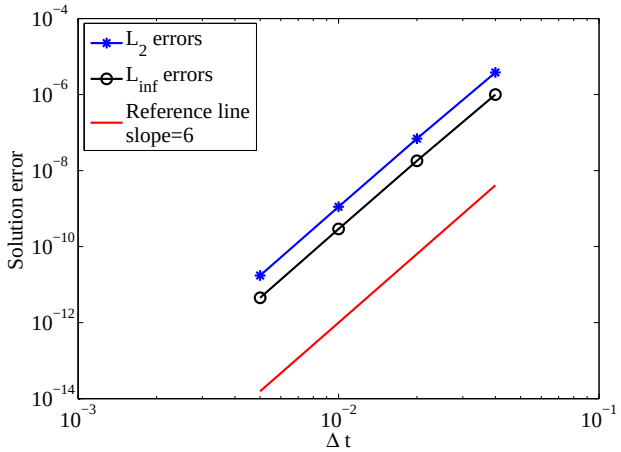

Figure 3: The convergence orders in time of scheme (3.13) with $r=3$, $k=6$ at $t=1$ ($\Delta x=0.2$).

Table 7: Maximum energy errors of scheme (3.13) in $t\in[0,10]$ with $r=3$.

Δx	Δt	$k=3$	$k=6$
1	0.1	4.5699×10^{-6}	9.0549×10^{-14}
1	0.05	7.2984×10^{-8}	5.0625×10^{-14}
0.8	0.08	1.5379×10^{-5}	7.1054×10^{-14}
0.8	0.04	2.4682×10^{-7}	1.3323×10^{-14}
0.4	0.04	1.3099×10^{-8}	4.5297×10^{-14}
0.4	0.02	2.1712×10^{-10}	4.0856×10^{-14}
0.2	0.01	1.2257×10^{-13}	1.1902×10^{-13}

4.2 Collision of two solitary waves

In this experiment, various collision behaviors between two solitons described by the CNLS equations (1.1) are simulated and the initial conditions are taken as

$$\begin{cases} \phi(x,0)=\sqrt{2}a_1\mathrm{sech}(a_1x+b/2)\exp(\mathrm{i}v_1x/4), \\ \psi(x,0)=\sqrt{2}a_2\mathrm{sech}(a_2x-b/2)\exp(-\mathrm{i}v_2x/4), \end{cases} \tag{4.2}$$

where $-40\leqslant x\leqslant 40$, $b=20$. a_i and v_i $(i=1,2)$ are amplitude and velocity parameters, respectively. Although considering the same initial values, different nonlinear constants β will impact the evolutions of the collision in different way.

4.2.1 Elastic collision

According to [17], when $\beta=1$, the collision of solitary waves is elastic. In Fig. 4, the evolution of the collision with $a_1=1.5$, $a_2=1$, $v_1=v_2=1$ and the variation of energy

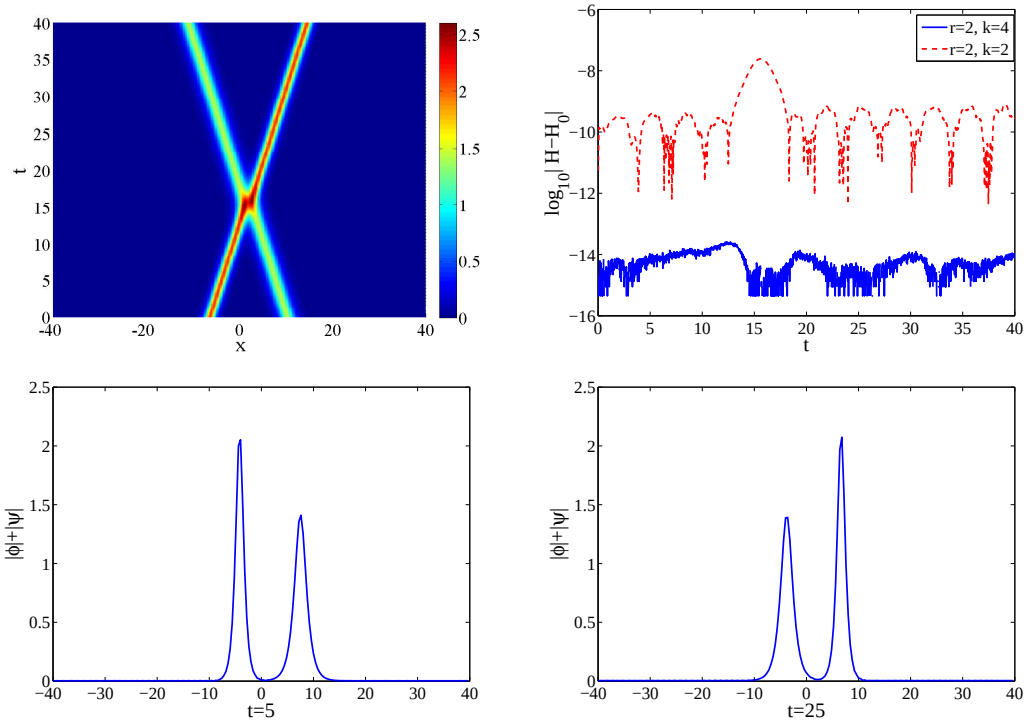

Figure 4: The evolution of elastic collision of two solitons obtained from scheme (3.13) with different amplitudes ($a_1=1.5$, $a_2=1$) (left top). The variation of energy errors in $t\in[0,40]$ (right top). The waveforms of the CNLS equations with the initial conditions (4.2) at $t=5$ (left bottom) and $t=25$ (right bottom).

errors are depicted. Obviously, after collision, the two solitons still move forward in the same direction and velocity, meanwhile, the amplitudes remain unchanged. The energy error of energy-preserving scheme ($r=2$, $k=4$) is around 10^{-14} all the time, but the energy error of the other scheme ($r=2$, $k=2$) can only reach the magnitude of 10^{-10}. Then we let $a_1=a_2=1$, $v_1=2$ $v_2=1$. The collision of solitary waves with different velocities are shown in Fig. 5. It can be seen that the two solitons also can keep the directions, velocities and amplitudes as before. Furthermore, the top right picture in Fig. 5 reflects the effectiveness of energy-preserving scheme, especially when the collision happens. Next, in order to compare the cost of CPU time, scheme (3.15) is applied to simulate the collision. From Table 8, we find the HOCM indeed has better computing efficiency and also can preserve energy very well.

4.2.2 Inelastic collision

For the inelastic collision, we only take $r=2$, $k=4$, $\Delta t=0.01$, $\Delta x=0.2$ in schemes (3.13) and (3.15), and set $a_1=a_2=1$, $v_1=v_2=1$ in initial conditions (4.2). Letting $\beta=2/3$, $\beta=2$ and $\beta=3$, the corresponding simulations of the inelastic collision are all displayed in Fig. 6. Obviously, with different β, the evolutions of the waveform are completely

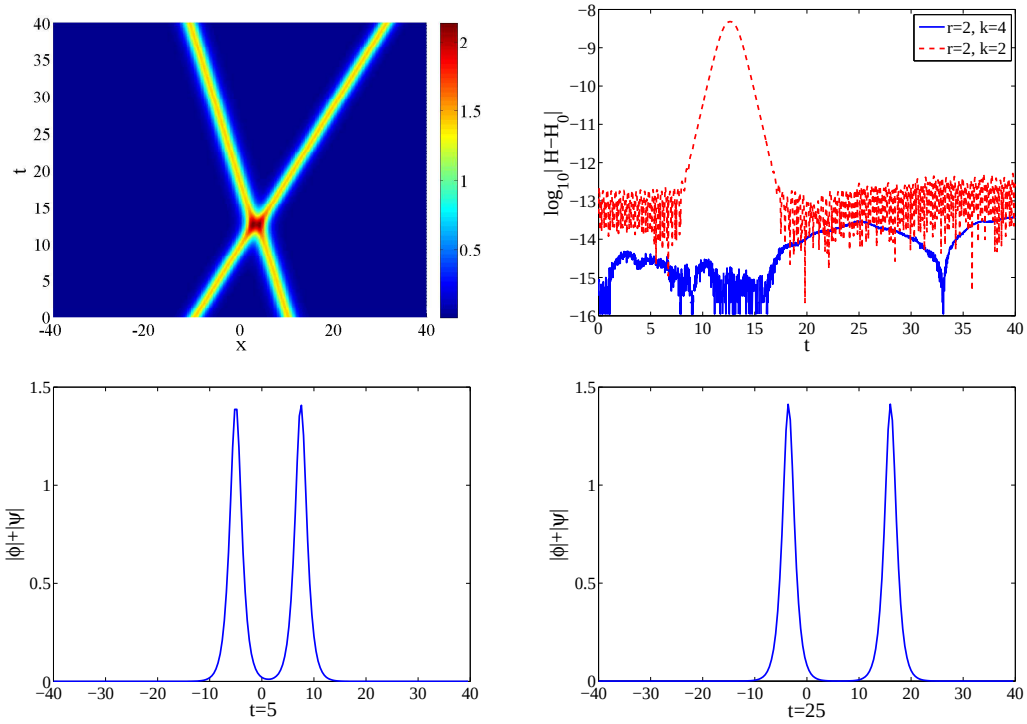

Figure 5: The evolution of elastic collision of two solitons obtained from scheme (3.13) with different velocities ($v_1=2$, $v_2=1$) (left top). The variation of energy errors in $t\in[0,40]$ (right top). The waveforms of the CNLS equations with the initial conditions (4.2) at $t=5$ (left bottom) and $t=25$ (right bottom).

Table 8: Maximum energy errors and CPU times of schemes (3.13) and (3.15) in $t\in[0,40]$ ($\Delta x=0.8$, $\Delta t=0.04$).

HBVM(k,r)		HOCM		FPM	
k	r	energy error	CPU time	energy error	CPU time
2	1	5.3180×10^{-13}	5.03	6.7857×10^{-13}	6.79
4	2	7.0610×10^{-14}	7.96	1.1546×10^{-14}	10.07
6	3	2.2204×10^{-14}	10.91	5.9952×10^{-15}	12.88

different after the collision: (i) when $\beta=2/3$, the two solitons are trapped with each other; (ii) when $\beta=2$, the two solitons propagates with small shock; (iii) and when $\beta=3$, one new soliton is generated. Here, the simulated results of schemes (3.13) and (3.15) are almost the same and the energy errors of them also have little difference. Finally, by comparison of the two kinds of schemes with different β, an inference could be acquired from Table 9. When the coupling constant becomes larger, scheme (3.15), more obviously, appears its superiority in computing efficiency. Therefore, scheme (3.15) is more suitable to be applied for long time simulation.

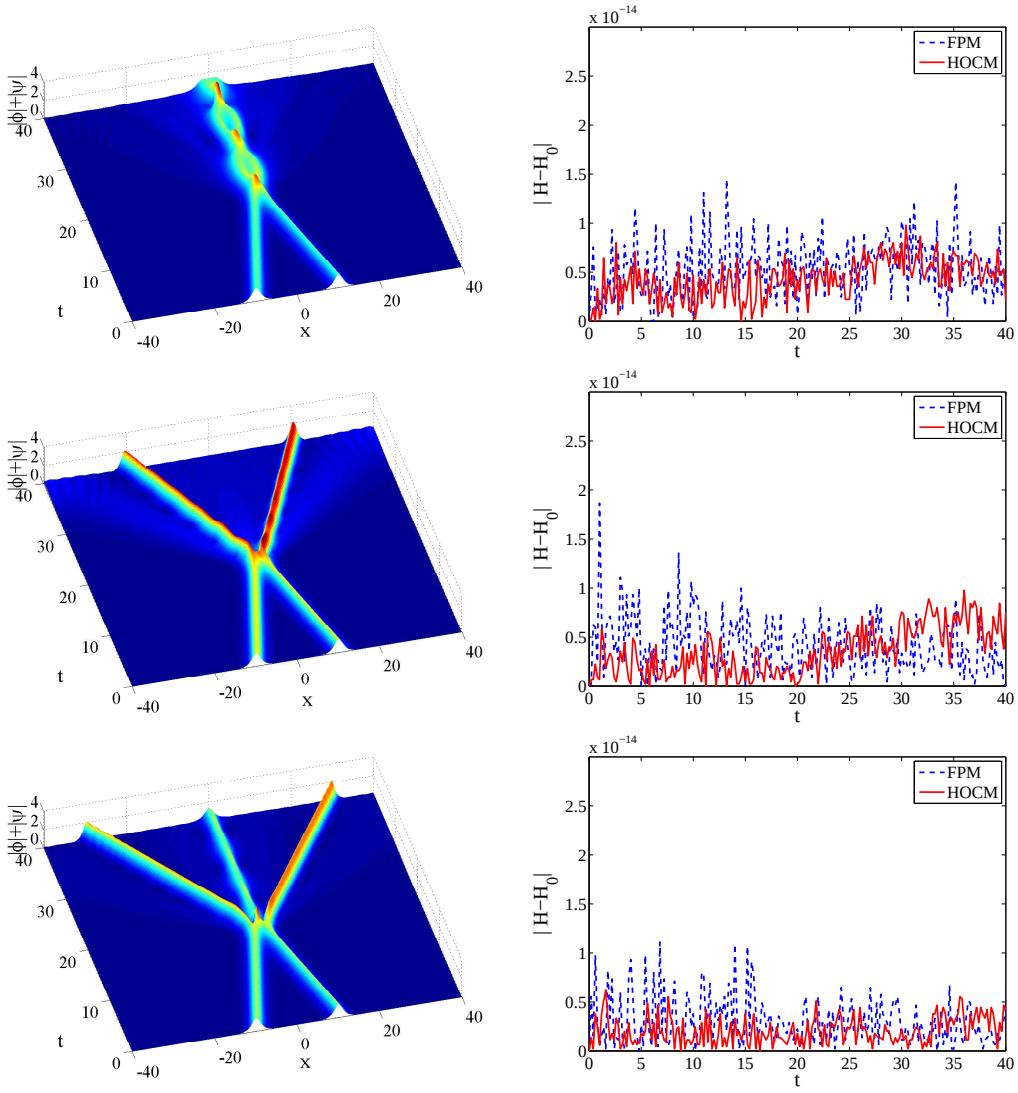

Figure 6: The evolution of the inelastic collision of two solitons with $\beta=2/3$, $\beta=2$ and $\beta=3$, and their variations of energy errors.

Table 9: CPU times in $t\in[0,40]$ of schemes (3.13) and (3.15) with $r=2$, $k=4$ ($\Delta x=0.2$, $\Delta t=0.01$).

	$\beta=\frac{2}{3}$	$\beta=1$	$\beta=2$	$\beta=3$
FPM	113.56	112.96	145.48	171.43
HOCM	105.00	106.84	109.05	112.18

5 Conclusion

In this paper, we propose two kinds of energy-preserving schemes, based on the HBVMs, the FPM and the HOCM, to solve the CNLS equations. It can be theoretically verified

that schemes (3.13) and (3.15) have $2r$ order convergent rate in time and could preserve corresponding discrete energy exactly for $k \geq 2r$. Numerical results fully indicate that both of the schemes are effective in numerical simulation. By comparison with the situation of $k = r$, the energy-preserving characters of schemes (3.13) and (3.15) with $k = 2r$ can be evidently confirmed. Moreover, the schemes using the FPM or the HOCM have their own advantages. It can be seen that the numerical accuracy of scheme (3.13) is higher, whereas the computational efficiency of scheme (3.15) performs better.

Acknowledgments

This work is supported by the Natural Science Foundation of China (Grant Nos. 11571366, 11501570), the China Postdoctoral Science Foundation (Grant No. 2017M613362) and the Open Foundation of State Key Laboratory of High Performance Computing of China.

References

[1] D. I. Benney, A. C. Newell, Sequential time closures for interacting random waves, Studies in Applied Mathematics, 46(1967),363-393.
[2] W. Z. Bao, The nonlinear Schrödinger equation and applications in Bose-Einstein condensation and plasma physics, Dynamics in models Of coarsening, Coagulation, Condensation and Quantization. 2007:141-239.
[3] W. Z. Bao, Q. L. Tang, Z. G. Xu, Numerical methods and comparison for computing dark and bright solitons in the nonlinear Schrödinger equation, Journal of Computational Physics, 235(2013),423-445.
[4] A. Borhanifar, R. Abazari, Numerical study of nonlinear Schrödinger and coupled Schrödinger equations by differential transformation method, Optics Communications, 283(2010),2026-2031.
[5] L. Brugnano, F. Iavernaro, D. Trigiante, A note on the efficient implementation of Hamiltonian BVMs, Journal of Computational and Applied Mathematics, 236(2012),375-383.
[6] L. Brugnano, F. Iavernaro, D. Trigiante, Hamiltonian Boundary Value Methods (Energy Preserving Discrete Line Integral Methods), Journal of Numerical Analysis, Industrial and Applied Mathematics, 5,1-2 (2010) 17-37.
[7] L. Brugnano, F. Iavernaro, D. Trigiante, A simple framework for the derivation and analysis of effective one-step methods for ODEs, Applied Mathematics and Computation, 218(2012),8475-8485.
[8] L.Brugnano, Y.Sun, Multiple invariants conserving Runge-Kutta type methods for Hamiltonian problems, Numerical Algorithms 65 (2014) 611-632.
[9] L. Brugnano, G. Frasca Caccia, F. Iavernaro, Energy conservation issues in the numerical solution of the semilinear wave equation, Applied Mathematics and Computation, 270(2015),842-870.
[10] L. Brugnano, F. Iavernaro, Line Integral Methods for Conservative Problems, Chapman et Hall/CRC, Boca Raton, FL, 2016.
[11] L.Barletti, L.Brugnano, G.Frasca Caccia, F.Iavernaro, Recent advances in the numerical solution of Hamiltonian partial differential equations. AIP Conference Proc. 1776, 020002 (2016).

[12] L. Barletti, L. Brugnano, G. Frasca Caccia, F. Iavernaro, Solving the nonlinear Schrödinger equation using energy conserving Hamiltonian boundary value methods. AIP Conference Proc.1863,160002(2017).
[13] L. Barletti, L. Brugnano, G. Frasca Caccia, F. Iavernaro, Energy-conserving methods for the nonlinear Schrödinger equation, Applied Mathematics and Computation, 318(2018),3-18.
[14] J. B. Chen, M. Z. Qin, Multi-symplectic Fourier pseudospectral method for the nonlinear Schrödinger equation, Electronic Transactions on Numerical Analysis, 12(2001),193-204.
[15] Y. M. Chen, H. J. Zhu, S. H. Song, Multi-symplectic splitting method for the coupled nonlinear Schrödinger equation, Computer Physics Communications, 181(2010),1231-1241.
[16] E. Celledoni, V. Grimm, R. I. Mclachlan, D. I. Mclaren, D. O'Neale, B. Owren, G. R. W. Quispel, Preserving energy resp. dissipation in numerical PDEs using the Average Vector Field method, Journal of Computational Physics, 230(2012),6770-6789.
[17] J. X. Cai, Y. S. Wang, H. Liang, Local energy-preserving and momentum-preserving algorithms for coupled nonlinear Schrödinger system, Journal of Computational Physics, 239(2013),30-50.
[18] J. L. Hong, C. Li, Multi-symplectic Runge-Kutta methods for nonlinear Dirac equations, Journal of Computational Physics, 211(2006),448-472.
[19] E. Infeld, G. Rowlands, Nonlinear Waves, Solitons and Chaos, Cambridge University Press, Cambridge, 1990.
[20] M. S. Ismail, T. R. Taha, A linearly implicit conservative scheme for the coupled nonlinear Schrödinger equation. Mathematics and Computers in Simulation, 74(2008),302-311.
[21] M. S. Ismail, A fourth-order explicit schemes for the coupled nonlinear Schrödinger equation. Applied Mathematics and Computation, 196(2008),273-284.
[22] M. S. Ismail, Numerical solution of coupled nonlinear Schrödinger equation by Galerkin method. Mathematics and Computers in Simulation, 78(2008),532-547.
[23] Y.S. Kivshar, G.P. Agrawal, Optical Solitons: from fibers to photonic crystals, Academic Press, San Diego, 2003.
[24] A. Kurtinaitis, F. Ivanauskas, Finite difference solution methods for a system of the nonlinear Schrödinger equations, Nonlinear Analysis Modelling and Control, 9(2004),247-258.
[25] S. K. Lele, Compact finite difference schemes with spectral-like resolution, Journal of Computational Physics, 103(1992),16-42.
[26] R. I. Mclachlan, G. R. Quispel, N. Robidoux, Geometric Integration Using Discrete Gradients, Philosophical Transactions of the Royal Society B Biological Sciences, 357(1998),1021-1045.
[27] W. Miki, I. Takeshi, H. Masato, A coupled nonlinear Schrödinger equation and optical solitons[J]. Journal of the Physical Society of Japan, 2007, 61(7),2241-2245.
[28] Y. P. Ma, L. H. Kong, J. L. Hong, High-order compact splitting multisymplectic method for the coupled nonlinear Schrödinger equations, Computers and Mathematics with Applications, 61(2011),319-333.
[29] G. Q. Meng, Y. T. Gao, X. Yu, Y. J. Shen, Y. Qin, Multi-soliton solutions for the coupled nonlinear Schrödinger-type equations, Nonlinear Dynamics, 70(2012),609-617.
[30] X. Qian, S. H. Song, E. Gao, W. B. Li, Explicit multi-symplectic method for the Zakharov-Kuznetsov equation, Chinese Physics B, 21(2012),070206.
[31] Y. J. Sun, Quadratic invariants and multi-symplecticity of partitioned Runge-Kutta methods for Hamiltonian PDEs, Numerische Mathematik, 106(2007),691-715.
[32] Y. S. Wang, S. T. Li, New schemes for the coupled nonlinear Schrödinger equation, International Journal of Computer Mathematics, 87(2010),775-787.